



Aptamer-functionalized hydrogels promote bone healing by selectively recruiting endogenous bone marrow mesenchymal stem cells

Jiang-Shan Gong^{a,b,1}, Guo-Qiang Zhu^{a,b,1}, Yu Zhang^a, Bei Chen^a, Yi-Wei Liu^{a,b}, Hong-Ming Li^{a,b}, Ze-Hui He^{a,b}, Jing-Tao Zou^{a,b}, Yu-Xuan Qian^{a,b}, Sheng Zhu^{a,b}, Xin-Yue Hu^{a,b}, Shan-Shan Rao^{a,b,c}, Jia Cao^{a,b,c}, Hui Xie^{a,b,c,*}, Zhen-Xing Wang^{a,b,c,***}, Wei Du^{a,b,c,d,**}

^a Department of Orthopedics, Movement System Injury and Repair Research Center, Xiangya Hospital, Central South University, Changsha, Hunan, 410008, China

^b Hunan Key Laboratory of Angiomedicine, Changsha, Hunan, 410008, China

^c National Clinical Research Center for Geriatric Disorders (Xiangya Hospital), Changsha, Hunan, 410008, China

^d Department of Rehabilitation Medicine, Xiangya Hospital, Central South University, Changsha, Hunan, 410008, China

ARTICLE INFO

Keywords:

Aptamer
Hydrogel
Fracture
Endogenous
Bone marrow mesenchymal stem cells
In situ regeneration

ABSTRACT

Bone regeneration heavily relies on bone marrow mesenchymal stem cells (BMSCs). However, recruiting endogenous BMSCs for *in situ* bone regeneration remains challenging. In this study, we developed a novel BMSC-aptamer (BMSC-apt) functionalized hydrogel (BMSC-aptgel) and evaluated its functions in recruiting BMSCs and promoting bone regeneration. The functional hydrogels were synthesized between maleimide-terminated 4-arm polyethylene glycols (PEG) and thiol-flanked PEG crosslinker, allowing rapid *in situ* gel formation. The aldehyde group-modified BMSC-apt was covalently bonded to a thiol-flanked PEG crosslinker to produce high-density aptamer coverage on the hydrogel surface. *In vitro* and *in vivo* studies demonstrated that the BMSC-aptgel significantly increased BMSC recruitment, migration, osteogenic differentiation, and biocompatibility. *In vivo* fluorescence tomography imaging demonstrated that functionalized hydrogels effectively recruited DiR-labeled BMSCs at the fracture site. Consequently, a mouse femur fracture model significantly enhanced new bone formation and mineralization. The aggregated BMSCs stimulated bone regeneration by balancing osteogenic and osteoclastic activities and reduced the local inflammatory response via paracrine effects. This study's findings suggest that the BMSC-aptgel can be a promising and effective strategy for promoting *in situ* bone regeneration.

1. Introduction

Bone marrow mesenchymal stem cells (BMSCs) are a promising option for bone regeneration due to their high pluripotency [1,2]. Despite the increasing utilization of stem cells from various sources, their widespread application is still limited by deficiencies, such as stringent *in vitro* culture conditions, low *in vivo* cell survival efficiency, and potential ethical and tumorigenic risks [3,4]. Recruiting endogenous BMSCs for *in situ* bone regeneration can effectively avoid *in vitro* cell

manipulation and transplantation complications compared to the traditional method of *ex vivo* culture followed by *in vivo* transplantation [5–8]. Nevertheless, the complexity of the cellular components and the bone marrow microenvironment poses a challenge in specifically recruiting endogenous BMSCs for *in situ* bone regeneration [9,10]. Previous studies have indeed emphasized that the employment of specific antibodies targeting BMSC surface markers such as CD105, CD73, CD90, and CD106 often lacks precision [8,11,12]. The more recent identification of CD271 as a highly specific marker for BMSC isolation is

* Corresponding author. Department of Orthopedics, Movement System Injury and Repair Research Center, Xiangya Hospital, Central South University, Changsha, Hunan, 410008, China.

** Corresponding author. Department of Orthopedics, Movement System Injury and Repair Research Center, Xiangya Hospital, Central South University, Changsha, Hunan, 410008, China.

*** Corresponding author. Department of Orthopedics, Movement System Injury and Repair Research Center, Xiangya Hospital, Central South University, Changsha, Hunan, 410008, China.

E-mail addresses: huixie@csu.edu.cn (H. Xie), wangzx@csu.edu.cn (Z.-X. Wang), wzdnxy2016@csu.edu.cn (W. Du).

¹ Contributed equally to this work.

promising, and the deployment of CD271 antibody-functionalized microspheres has shown potential in bone regeneration [13]. Alternatively, chemoattractants, such as bone morphogenetic proteins (BMPs) or stromal cell-derived factor 1 (SDF-1), have been discovered to be equally effective in recruiting BMSCs. However, BMPs negatively affect bone regeneration, and SDF-1 is less selective, causing nonspecific recruitment of hemopoietic stem cells [14–17]. Accordingly, affinity molecules that can selectively recognize and bind to BMSCs while remaining safe for use must be explored.

According to previous research, nucleic acid aptamers are a notable type of synthesized ligands that can specifically bind to target molecules in the body [18]. Aptamers have the advantage of being chemically synthesized and therefore manufactured at a lower cost than other ligands, such as antibodies [19]. Additionally, aptamers with high affinity and specificity for their target molecules can be developed by employing stringent aptamer screening methods [20,21]. These features have raised interest in aptamer-functionalized hydrogels (aptgel), a new class of biomaterials. Aptgel has various potential applications, including protein delivery, cell capture, regenerative medicine, and molecular biosensing, by recognizing proteins, cells, and analytes [22,23]. For instance, hydrogels (Gel) loaded with aptamers for inflammatory cells recruit monocyte macrophages to enhance skin repair [24]. In our previous work, we employed the systematic evolution of ligands by exponential enrichment (SELEX) technology to screen a BMSC-specific aptamer (BMSC-apt) from the ssDNA sequence library [25,26]. However, the applicability of BMSC-aptgel for bone regeneration still requires further research to investigate whether it can effectively recruit endogenous BMSCs *in situ*.

This study aims to develop a biocompatible hydrogel for bone tissue engineering using maleimide-functionalized multiarm polyethylene glycol (PEG) and sulfhydryl-flanked PEG crosslinker via a Michael addition reaction. We modified BMSC-apt with an aldehyde group and reacted with the PEG crosslinker's thiol group to enhance its metabolic stability. The prepared BMSC-aptgel exhibited excellent efficacy in attracting and facilitating the attachment and proliferation of BMSCs, due to its unique grid-like structure. Endogenous BMSCs can promote osteogenic differentiation and play an anti-inflammatory role by secreting various paracrine factors, thus promoting *in vivo* bone regeneration. These findings pave the way for developing advanced biomaterials that selectively target and recruit specific cell types, providing a promising strategy for tissue regeneration beyond bone.

2. Materials and methods

2.1. The preparation of gel, BMSC-aptgel and Rd-aptgel

PEG-4ARM-MAL (20 kDa) and PEG-dithiol (HS-PEG-SH; 3.5 kDa) were provided by JenKem. The BMSC-specific aptamer (BMSC-apt, 5'-GAATTCAGTCGGACAGCGACGACGGTGA-TATGTCAAGGTCGTATGCACGA.

GTCAGAGGGATGGACGAATATCGTCTCCC-3') and a random sequence of nucleotides with the same number of bases (Rd-apt, 5'-ATCCA-GATGACG-CAN-NNNNNNNNNNNNNNNNNNNNNNNNNNNNNNNNNNNNNNNTGGA-CACGGTGGCTTAGT-3') were synthesized by Sangon Biotech.

For hydrogels (Gel) preparation, PEG-4ARM-MAL and PEG-dithiol were dissolved and mixed in PBS (pH = 7.4) at approximately 2:1 thiol to maleimide. Thiolate reacted with the alkene group in maleimide under base catalysis, forming stable bonds and assembling a polymer network via a Michael addition reaction. These reactions formed hydrogels within a short period (approximately 15 s) and were utilized in this experiment. The hydrogels were loaded with different concentrations of BMSC-apt to generate several BMSC-aptgel variants (200, 500, and 1,000 nM). The aldehyde group at the BMSC-apt terminus was

reacted with a thiol to achieve stable binding to the hydrogels. Similarly, the hydrogels were loaded with a random nucleotide sequence to create Rd-aptgel. BMSC-aptgel and Rd-aptgel were prepared at a concentration of 500 nM unless specified otherwise.

2.2. The loading efficiency of BMSC-aptgel

We exposed 250 nM, 500 nM, and 1,000 nM BMSC-aptgel to PBS for 30 days to determine the loading efficiency of BMSC-aptgel. Then, we removed any remaining BMSC-aptgel. Next, we crushed the samples, extracted their RNA, and performed a 33-cycle polymerase chain reaction (PCR) amplification. The resulting product was analyzed using agarose gel electrophoresis and a mixture of forward and reverse primers to ensure complete amplification. (forward primer: 5'-GAATTCAGTCGGACAGCG; reverse primer: 3'-CCCTCTGCTATAAGCAGGTAG).

2.3. Scanning electron microscopy (SEM)

The hydrogels were imaged using a scanning electron microscope (SEM, TESCAN MIRA, S6123) under an accelerating voltage of 5 kV.

2.4. Animal experiments

Experimental procedures and animal care were approved by Xiangya Hospital of Central South University's Ethics Review Committee (no. 202101008). All animal experiments were performed at the Department of Laboratory Animals, Central South University. The animal model used for surgical fracture was previously described [27]. We selected eight-week-old C57BL/6 male mice and administered general anesthesia (approximately 50 mg/kg) before a lateral skin incision on their right femur. Then, a blunt dissection was performed on the muscle to expose the mid-femur. A 23-gauge sterile pin was drilled into the distal femoral intercondylar notch. Then, the needle was penetrated along the medullary canal to the femur, and micro-scissors were used to interrupt the femur, causing a transverse fracture. These mice were randomly divided into five groups: Control (only fractures), Gel, BMSC-apt (only 500 nM aptamer dissolved in PBS), BMSC-aptgel, and Rd-aptgel. According to the different groups, 20 μ L of the corresponding intervention was administered directly to the fracture site of each mouse. After hydrogel formation at the fracture site in each group, the wound was sutured, and various individual signs of mice were observed. Following a three- or six-week treatment, the right femur was removed and fixed in 4 % paraformaldehyde in two batches.

2.5. Microcomputed tomography (μ CT) analysis

Mice right femora were dissected, fixed with 4 % paraformaldehyde for 24 h, and scanned using a vivaCT80 scanner (SCANCO Medical AG). The scanner's voltage and current were set to 55 kV and 145 μ A, with a pixel resolution of 11.4 μ m. The bone parameters were analyzed using image reconstruction (NRecon), data analysis (CTAn), and three-dimensional model visualization software (μ CTVol). A 3-dimensional microarchitecture analysis of the callus was performed using the distal femur. Approximately 700 slices were selected, with the fracture line placed in the center of the range. The region of interest (ROI) was meticulously scrutinized slice by slice, and a fixed threshold was used to distinguish mineralized tissue in the callus. The mineralized bone volume (BV), total callus tissue volume (TV), and BV/TV ratio of the callus were recorded and calculated.

2.6. *In vivo* fluorescent tracer imaging

This study used 1,1-dioctadecyl-3,3,3-tetramethylindotricarbocyanine iodide (DiR)-labeled BMSCs for near-infrared fluorescence *in vivo* distribution imaging. DiR and BMSCs were co-incubated at 37 $^{\circ}$ C with 5 % CO₂ for 30 min and then injected into the bone marrow cavity

of one femur at a concentration of approximately 1×10^5 cells in each mouse. Mice were subjected to femoral fracture modeling 2 h after injection and divided into Gel, BMSC-aptgel, and Rd-aptgel. At 6 and 12 h post-intervention, mice were anesthetized, and DiR fluorescence distribution was visualized using an in vivo imaging system (PerkinElmer, FMT4000) via fluorescence tomography after removal of the femur.

2.7. Histological and immunohistochemical analyses

The dissected femora were fixed with 4 % paraformaldehyde for 48 h and then decalcified in 10 % EDTA at a pH of 7.4 on a rocking bed for approximately seven days at 4 °C. Following graded dehydration with ethanol and paraffin embedding, bone samples were sliced longitudinally into 5- μ m-thick sections. Sagittal sections from the fracture area were stained with H&E (Servicebio, GP1031), SO/FG (Solarbio, G1371), and Trap (Servicebio, G1050) to conduct histological staining. Primary antibodies against rabbit anti-Nestin (Abcam, ab105389; 1: 200), OCN (Servicebio, GB11233; 1: 300), TNF- α (Servicebio, GB11188; 1: 800), IL-1 β (Servicebio, GB11113; 1: 400), and IL-6 (Servicebio, GB11117; 1: 400) were used, along with secondary antibodies for immunohistochemical staining (anti-rabbit, 1: 200). The staining images were all obtained at the fracture interface.

2.8. Biomechanical test

Three-point bending tests were conducted using a computer-controlled testing machine (Instron, 3343M1372) to assess the quality of fracture healing. The femur was positioned in the anterior-posterior direction of the inferior strut, with the lateral patella side facing up at a distance of 9 mm. The upper bar span was measured to be 5.5 mm. Then, a constant vertical compressive load was applied at 3 mm/min speed until failure. The maximum bending load (N) values were automatically recorded using the computer.

2.9. Cell culture

Sca-1⁺CD29⁺CD45⁻CD11b⁻ BMSCs were isolated from the bone marrow of C57BL/6 mice using flow cytometry and cultured in Alpha Modification of Minimum Essential Medium Eagle (α -MEM; Biological Industries). The mouse monocyte/macrophage cell line RAW264.7 was purchased from Procell and cultured in high-glucose Dulbecco's Modified Eagle Medium (DMEM; Biological Industries). Primary monocytes/macrophages from three-month-old male mice were cultured with macrophage colony-stimulating factor (M-CSF). All cells were cultured in a medium containing 10 % FBS (Gibco) and 100 unit/mL of penicillin and streptomycin (P/S) using a 37 °C, 5 % CO₂ humidified incubator.

2.10. Cell migration test

A 24-well transwell plate (Costar, USA) with an 8-mm aperture filter was utilized to measure cell migration. BMSCs (cell density: 1.0×10^5 cells per well) were cultured in the upper chamber with a complete medium (containing basal medium, 1 % P/S, and 10 % FBS), while hydrogels or BMSC-aptgel were added into the lower chamber. After co-culturing the cells for 24 h, the culture medium was removed from the cells, washed with PBS, and fixed with 4 % paraformaldehyde for 10 min. Subsequently, the cells on the top membrane surface were eliminated, and 500 μ L of 0.1 % crystalline violet buffer was added to every well for cells on the lower surface for 10 min. After three washes, positively stained cells were counted under an inverted microscope (Leica).

2.11. Osteogenesis induction

We seeded primary BMSCs in 48-well plates at a density of 2×10^5 cells per well. The experimental group was treated with Eagle's Minimal

Essential Medium (EMEM; Biological Industries) supplemented with osteogenic induction factor (10 nM dexamethasone, 5 mM β -phosphoglycerol, and 50 μ g/mL ascorbic acid) and 500 nM BMSC-aptgel. A positive control (PC) and Gel group were cultured in EMEM containing osteogenic induction factor, while a negative control group (NC) received EMEM without osteogenic induction factor or BMSC-apt. Each group had three accessory wells. After seven days, an inverted microscope (Leica, DMI4000B) was used to image and count BMSC osteogenic differentiation in each group. Cell supernatants were collected from each group during cell culture, and supernatant ALP activity was detected using Alkaline Phosphatase Assay Kit (Beyontime, P0321). Subsequently, mineralization of the cellular matrix was evaluated by fixing the differentiated bone marrow stromal cells with 4 % paraformaldehyde and staining them with 2 % Alizarin Red S (Sigma-Aldrich, a5553) at pH 4.2.

2.12. Osteoclastogenesis induction

We seeded the murine monocyte/macrophage cell line RAW264.7 cells per well in 48-well plates at a density of 2×10^3 . The experimental group was treated with DMEM supplemented with 100 ng/mL of osteoclastogenesis induction factor RANKL (PeproTech, AF-310-01) and 500 nM of BMSC-apt, while the positive and negative control groups received an equal volume of DMEM with RANKL and DMEM without osteogenic induction factor or BMSC-apt, respectively. Three replicates were performed for each group. After 12-day culture, fixed cells were stained using the Trap staining kit (Sigma-Aldrich, 387A) and observed under an inverted microscope (Leica, DMI4000B) to quantify osteoclastogenesis differentiation (three or more cell nuclei per cluster).

2.13. Calcein-AM/PI staining

The BMSCs (cell density: 2×10^4 cells per well) were plated in a 24-well plate and treated with control, Gel, or BMSC-aptgel for three days. The BMSCs were washed with assay buffer and incubated with calcein-AM and PI solution (Yeasen, 40747ES76) at 37 °C for 30 min. Subsequently, the BMSCs were washed with PBS, resuspended in assay buffer and placed on glass slides. Images were taken using Zeiss Fluorescence Microscope (Jena, Germany). The dead cells (PI positive) and live cells (calcein-AM positive) were counted.

2.14. Quantitative real-time PCR analysis

Total RNA was extracted from Formalin-Fixed Paraffin Embedded (FFPE) fractured bone tissue using FFPE Tissue RNA Kit (G3642, Servicebio) and cDNA was synthesized from 1 μ g of total RNA using the All-in-One cDNA Synthesis SuperMix (Biotool, Houston, USA). The cDNA was amplified using 2 \times SYBR Green qRT-PCR Master Mix (Bimake, Houston, USA) on an FTC-3000 real-time PCR system (Funglyn Biotech Inc, Toronto, Canada). Relative gene expressions were measured by the $2^{-\Delta\Delta CT}$ method with reference to GAPDH. The primer sequences for the mouse used in this study were as follows: *Runx2*: forward, 5'-CGCCACCACTCACTACCACAC-3', and reverse, 5'-TGGATTAA-TAGCGTGTCTGCC-3'; *Bgalp*: forward, 5'-TTCTGCTCACTCTGTGACCC-3', and reverse, 5'-CTGATAGCTC GTCACAAGCAGG-3'; *Col1a*: forward, 5'-CTGACTGGAAGAGCGGAGAG-3', and reverse, 5'-CGGCTGAGTAGG-GAACACAC-3'; *GAPDH*: 5'-CACCA TGGAGAAGCCGGGG-3', and reverse, 5'-GACGGACACATTGGGGGTAG-3'.

2.15. Statistical analysis

The mean and standard deviation (SD) of continuous variables were denoted in GraphPad Prism 9. One-way or two-way ANOVA with Bonferroni's post hoc analysis was used for statistical analysis. For all experiments, $P < 0.05$ was considered statistically significant.

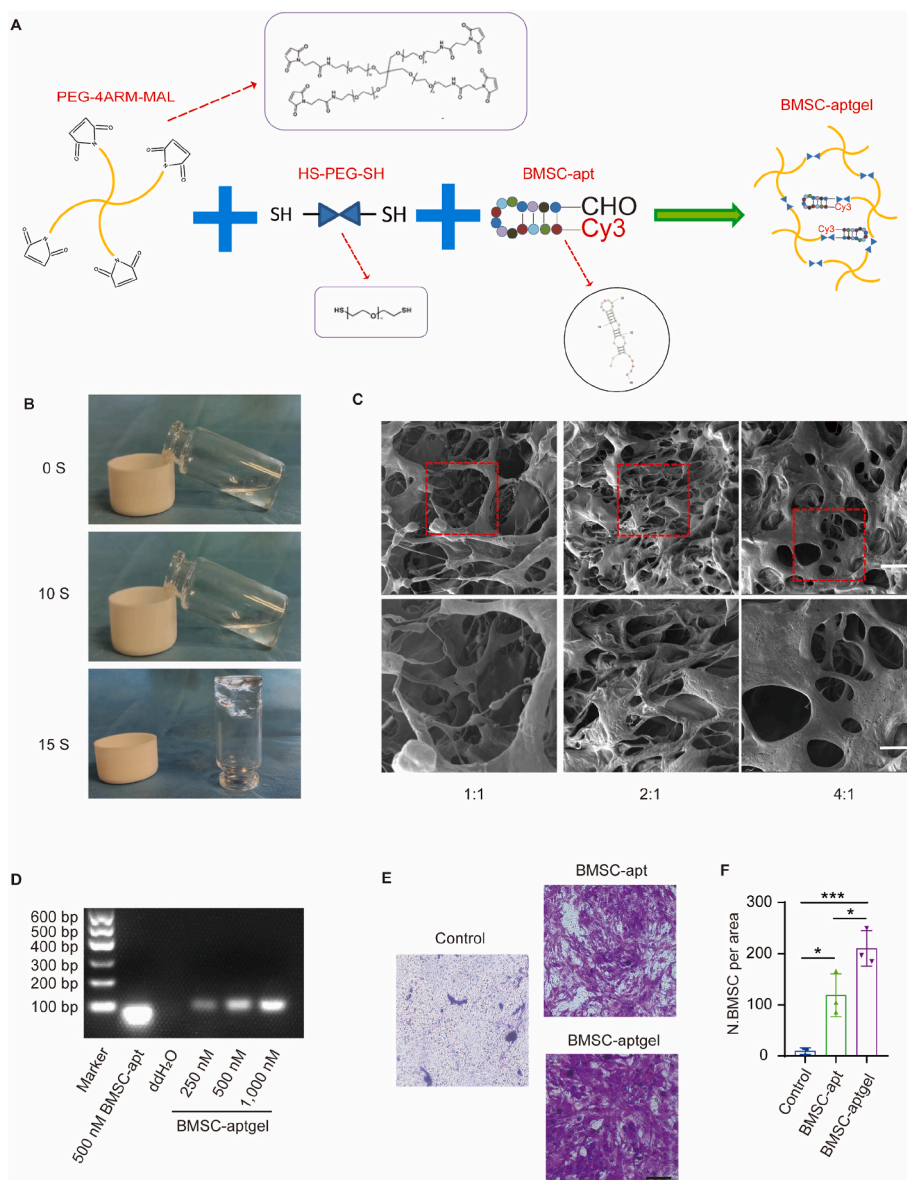


Fig. 1. BMSC-aptgel characterization and in vitro cell capture.

A) Diagram of the conjugation procedures of PEG hydrogel containing the BMSC-specific aptamer. B) Representative images of the BMSC-aptgel formation process at different time points. C) Representative SEM images of the BMSC-aptgel with different proportions of PEG-4ARM-MAL and HS-PEG-SH. Scale bars: 200 μm (upper), 100 μm (lower). D) The remaining aptamer in the hydrogel was detected by PCR after immersing the BMSC-aptgel of 250 nM, 500 nM, and 1,000 nM in PBS for 30 days. E, F) Representative images of the transwell migration assay (E) and the numbers of crystal violet-stained migrated cells. * $P < 0.05$, *** $P < 0.001$.

3. Results and discussion

3.1. BMSC-aptgel characterization and in vitro cell capture

The BMSC-aptgel skeleton consisted of a four-arm PEG with a terminal maleimide group (PEG-4ARM-MAL). This platform enabled the construction of structurally defined hydrogels with independently tunable polymer density, adhesive peptide, and crosslinker [28,29]. While gelatin and hyaluronic acid are indeed known for their bone regenerative properties [30,31], PEG hydrogel offers distinct advantages. Firstly, PEG is a biocompatible and non-toxic material that has been widely used in various medical applications. Secondly, PEG hydrogel has excellent mechanical properties, allowing it to withstand the mechanical stresses present in bone tissue. Additionally, its chemical reactivity makes it amenable to various modifications, enabling the incorporation of functional groups that can promote bone regeneration. Furthermore, PEG hydrogel can be designed to have a porous structure,

which facilitates cell adhesion, proliferation, and differentiation [32–35]. *In situ*, dithiol PEG (HS-PEG-SH) reacted with the maleimide group to form a PEG hydrogel. It formed a dynamic covalent bond with the thiol group of the PEG crosslinker by modifying the aldehyde group at the 5' terminus of the BMSC-specific aptamer (BMSC-apt), resulting in functional aptamer hydrogels (BMSC-aptgel) that could recruit BMSCs (Fig. 1A).

In this study, we utilized maleimide-modified 4-arm functional PEG (PEG-4ARM-MAL) and a thiol-flanked PEG crosslinker that retained the desirable properties of PEG-based hydrogels. Fig. 1B demonstrates that the hydrogel gelation time is fast at only 15 s. Scanning electron microscopy (SEM) images revealed the hydrogel's highly porous and physically stable internal structure at a PEG-4ARM-MAL to HS-PEG-SH ratio of 2:1 (Fig. 1C). *In situ* rapid gel formation coupled with the porous structure improved physical support for post-surgical fracture stability and promoted the attraction of BMSCs for bone regeneration at the fracture site. Furthermore, the excellent ultrarapid formation ability

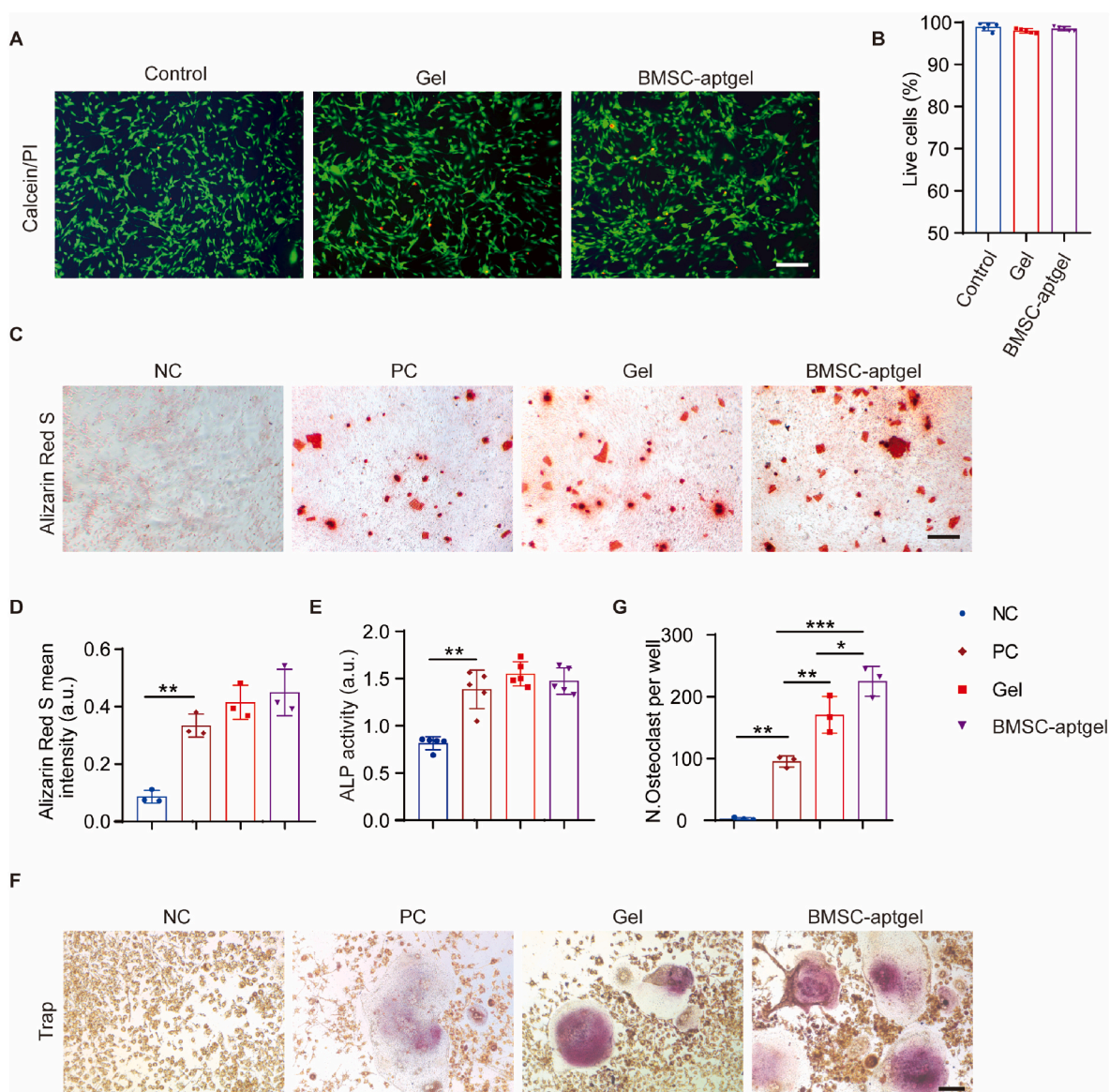


Fig. 2. BMSC-aptgel maintains BMSC activities in vitro.

A, B) Representative images of calcein (green; live cells) and PI (red; dead cells) staining of BMSCs in growth condition medium for 3 days (A), and the percentages of live cells (B). Scale bar: 200 μ m, n = 5 per group. C-E) Representative images of Alizarin Red S staining of mineral deposition of BMSCs in osteogenic conditioned medium (C), and the quantitative analysis of the mineralization intensity (D) and ALP activity (E). Scale bar: 200 μ m, n = 3 (D) or 5 (E) per group. F, G) Representative images of Trap staining of osteoclasts of RAW264.7 cells in osteoclastic conditioned medium (F), and the quantification analysis of osteoclast number (G). Scale bar: 100 μ m, n = 3 per group. * $P < 0.05$, ** $P < 0.01$, *** $P < 0.001$; NC, negative control; PC, positive control.

of the hydrogels greatly reduced the operation time of fracture internal fixation and minimized the risk of infection related to incision exposure because the duration of surgery was directly associated with the risk of infection in fracture surgery [36]. We prepared BMSC-aptgel using specific aptamers at three different concentrations (250 nM, 500 nM, and 1,000 nM) and immersed them in PBS to determine the optimal aptamer concentration for sustained standby. After 30 days, the supernatants were collected for PCR detection. Our data indicated that the 500 nM aptamer concentration supernatant remained strongly positive (Fig. 1D). Therefore, we selected the hydrogel with an aptamer concentration of 500 nM for further research. The transwell assay was conducted to demonstrate that the function of BMSC-aptgel for BMSC recruitment was mediated by BMSC-apt. The BMSC-aptgel group captured a higher number of BMSCs than the control and free BMSC-apt groups, with no significant difference between the latter two (Fig. 1E and F).

These initial findings suggested that the BMSC-aptgel had excellent sustained release properties and provided adequate physical space for the recruitment of significant numbers of BMSCs.

3.2. BMSC-aptgel maintains BMSC activities in vitro

Next, we evaluated the impact of BMSC-aptgel on cytocompatibility, osteogenic potential, and osteoclastogenic capacity in vitro. To demonstrate that its toxicity was comparable to that of an empty hydrogel, equivalent quantities of BMSCs were seeded on normal plastic plates, PEG gel-, or BMSC-aptgel-coated plates. Calcein-AM/PI staining results revealed that the BMSC-aptgel group had an impressive cell survival rate of approximately 98%–99% (Calcein-positive, green staining), with few instances of cell death (PI-positive, red staining) (Fig. 2A and B). Alizarin red S (ARS) staining presented that the BMSCs cultured on BMSC-aptgel-coated plates have a slight increase in a

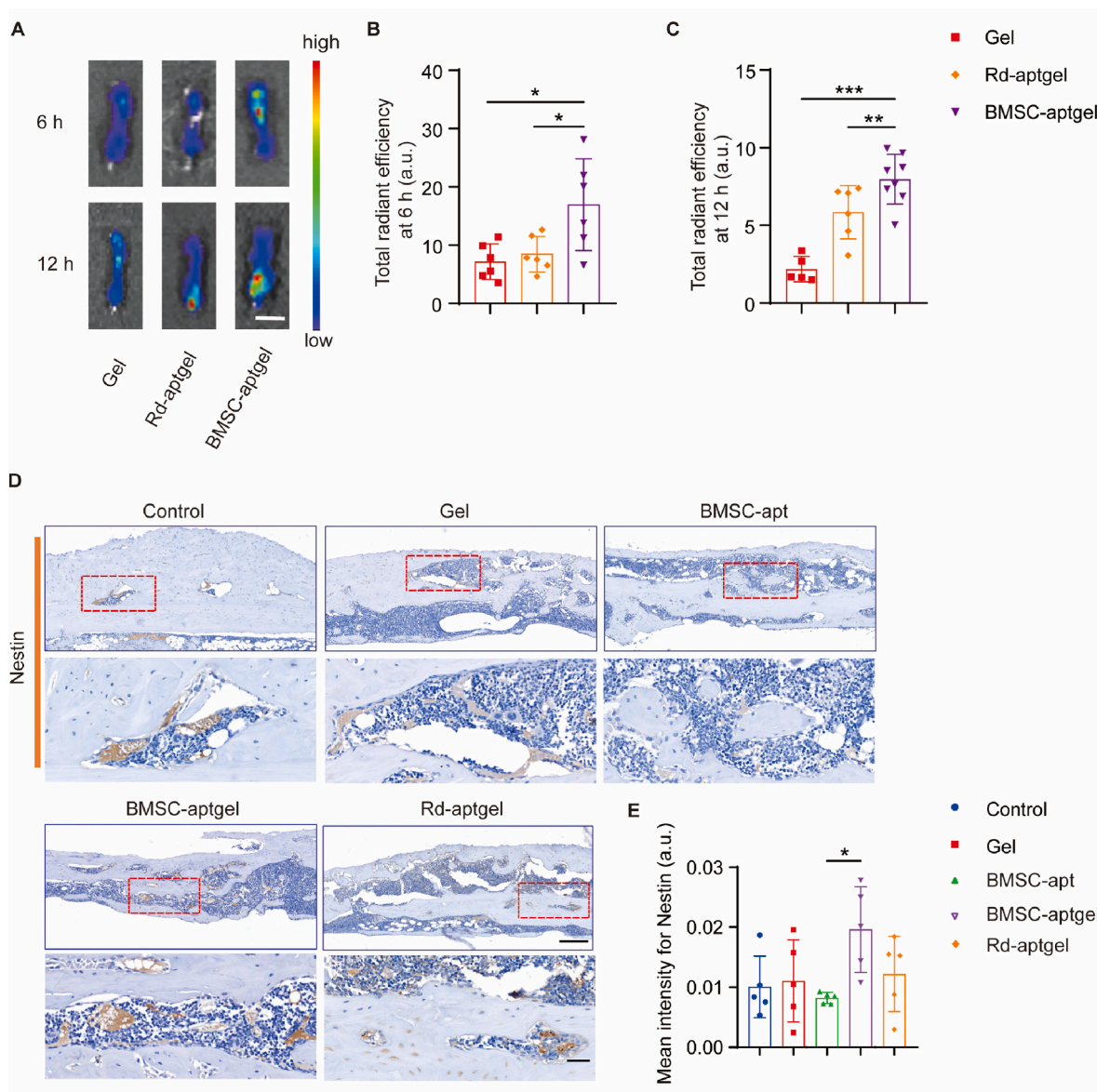


Fig. 3. BMSC-aptgel recruits BMSCs in vivo.

A) Representative fluorescence tomography images of BMSC-DiR in isolated fractured femora of mice at different time points. Scale bar: 5 mm. B, C) Quantification analysis of fluorescence intensity after 6 h (B; n = 6 per group) or 12 h (C; Gel: n = 5, Rd-aptgel: n = 6, BMSC-aptgel: n = 8). D, E) Representative images of immunohistochemical staining of Nestin at the fracture area (D), and quantitative analyses of Nestin intensity (E). Scale bars: 100 μm or 50 μm (zoomed). n = 5 per group. **P* < 0.05, ***P* < 0.01, ****P* < 0.001.

mineral deposition. However, this increase was not statistically significant compared to the osteogenic-induced positive control (PC) or Gel groups (Fig. 2C and D). Additionally, mineral deposition and early markers, such as alkaline phosphatase (ALP), are often used to assess the osteogenic differentiation of BMSCs [37]. The supernatants were collected to perform ALP activity assays. Consistent with the ARS staining, the ALP activity of the BMSC-aptgel group did not rise significantly compared to the Gel group (Fig. 2E). We also analyzed its effects on the differentiation of osteoclasts to evaluate the impact of BMSC-aptgel on the osteoblastic-osteoclastic balance comprehensively. Tartrate-resistant acid phosphatase (Trap) staining revealed that BMSC-aptgel significantly promoted osteoclast differentiation compared to cells cultured on the Gel and Control groups (Fig. 2F and G).

These findings suggested that BMSC-aptgel could preserve the osteogenic differentiation of BMSCs.

3.3. BMSC-aptgel recruits BMSCs in vivo

In the in vivo imaging experiment, our aim was to verify the efficacy of BMSC-aptgel in recruiting BMSCs at the fracture site. To achieve this, we compared it with a hydrogel group and a hydrogel group containing a randomly sequenced aptamer. Our study evaluated the capacity of BMSC-aptgel to recruit BMSCs in vivo by developing a mouse femur fracture model and treating it with the BMSC-aptgel. Additionally, an equal number of random nucleotide sequences were utilized to create a hydrogel (Rd-aptgel) to eliminate any potential influence of nucleotide bases. BMSCs were incubated with the lipophilic deep red fluorescent dye DiR to acquire BMSC-DiR complexes for later use. Subsequently, BMSC-DiR was locally administered to the mouse femur's bone marrow cavity via injection. A mouse femoral fracture was created under general anesthesia 2 h after the injection. Then, inert Gel, Rd-aptgel, and BMSC-aptgel were added to the fracture site. After 6 or 12 h, the treated fractured femur was dissected to examine BMSCs-DiR aggregation at

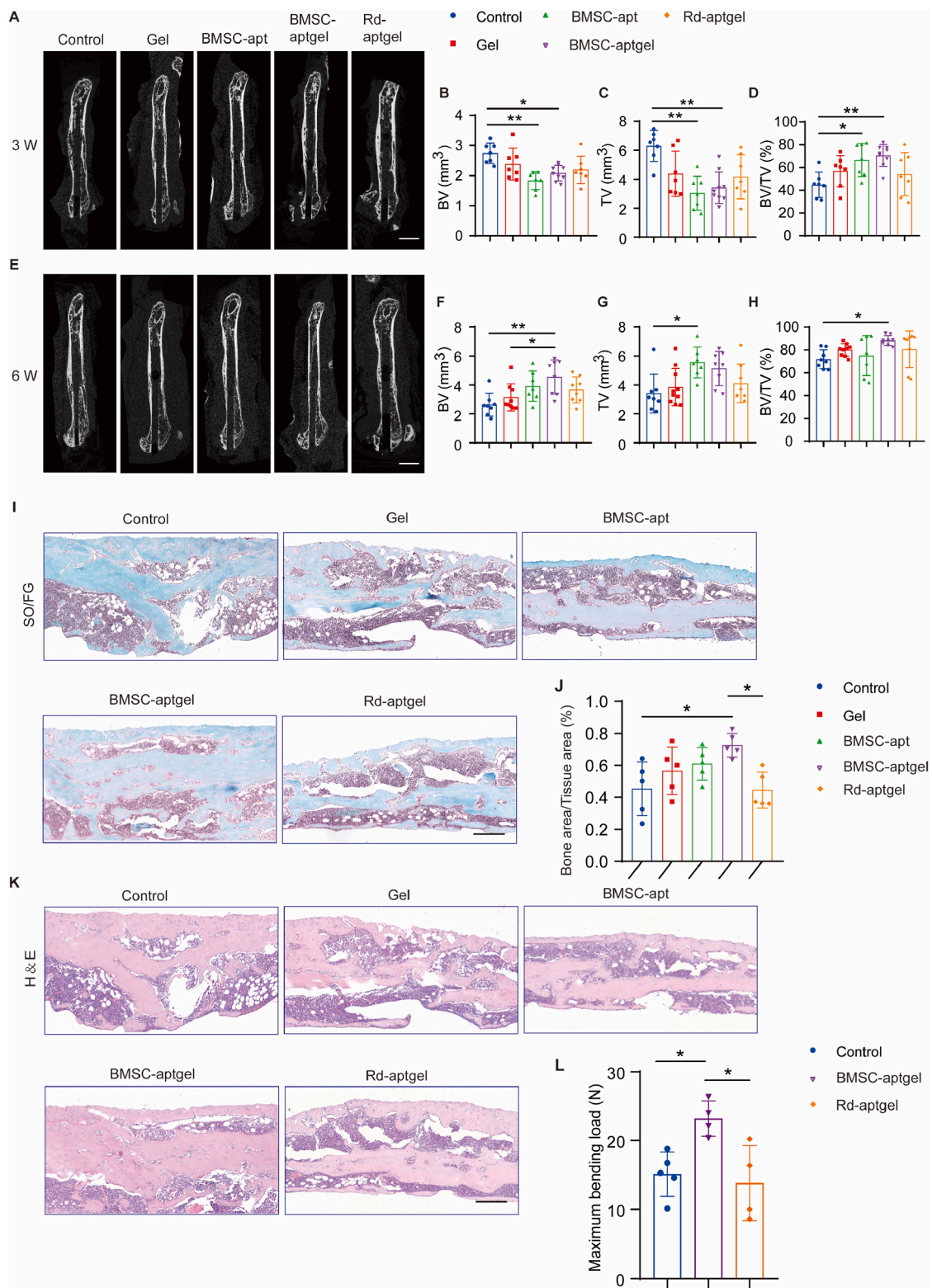


Fig. 4. BMSC-aptgel accelerates fracture healing in vivo.

A) Representative μ CT images of fractured femora after different treatments at 3 weeks. Scale bar: 5 mm. B-D) Quantitative analyses of BV (B), TV (C), and BV/TV (D) of fractured femora at 3 weeks. Control: n = 7, Gel: n = 7, BMSC-apt: n = 7, BMSC-aptgel: n = 9, Rd-aptgel: n = 7. E) Representative μ CT images of fractured femora after different treatments at 6 weeks. Scale bar: 5 mm. F-H) Quantitative analyses of BV (F), TV (G), and BV/TV (H) of fractured femora at 6 weeks. Control: n = 8, Gel: n = 9, BMSC-apt: n = 7, BMSC-aptgel: n = 8, Rd-aptgel: n = 8. I, J) Representative images of SO/FG staining (I) and quantitative analyses (J) of the positively stained area at the fracture area. Scale bar: 250 μ m, n = 5 per group. K) Representative images of H&E staining of the fracture area. Scale bar: 250 μ m. L) Three-point bending measurement of femoral ultimate load at 6 weeks. Control: n = 5, Gel: n = 4, BMSC-aptgel: n = 4, Rd-aptgel: n = 4. * P < 0.05, ** P < 0.01, *** P < 0.001.

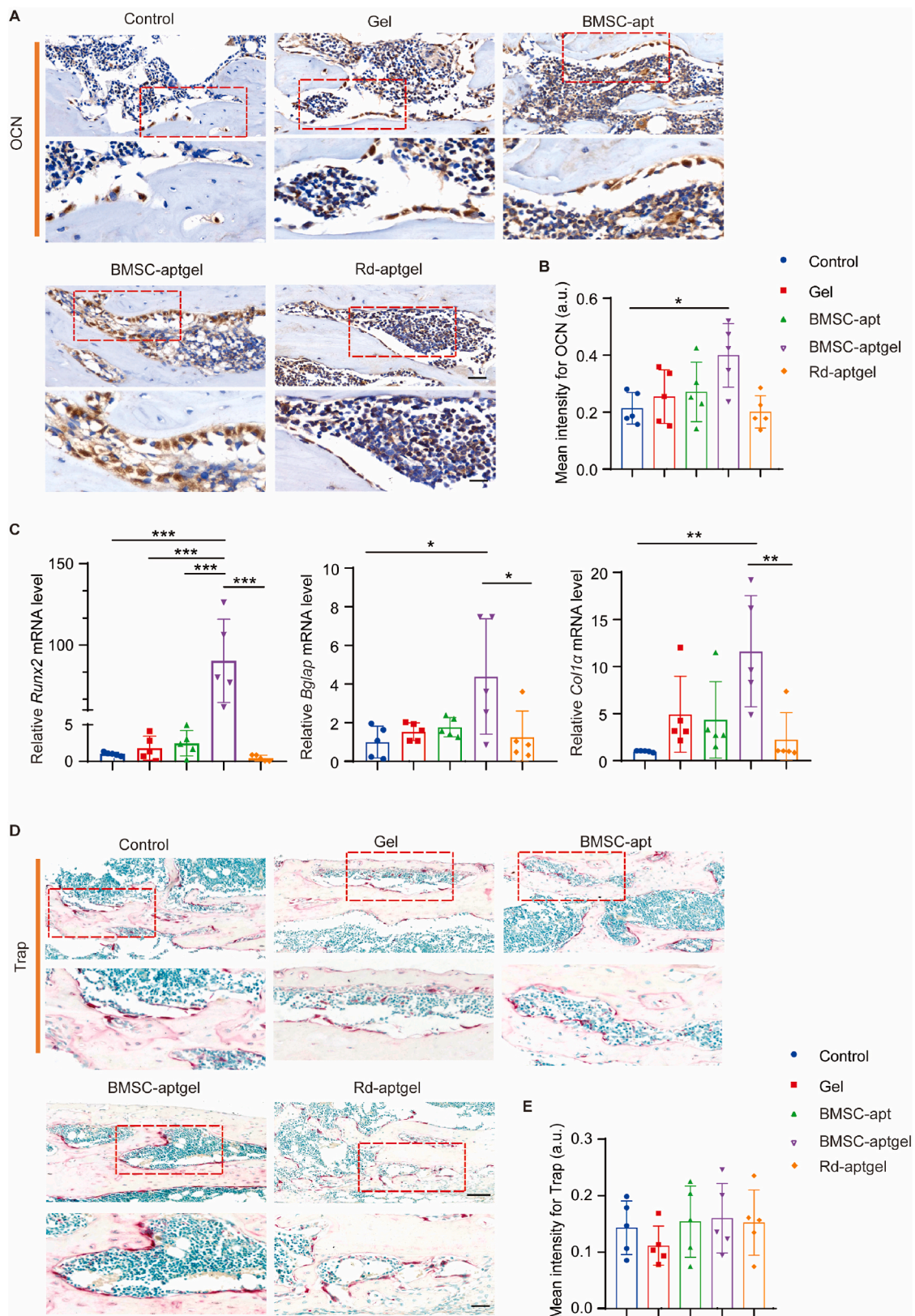


Fig. 5. BMSC-aptgel enhances osteoblastic differentiation in vivo. A, B) Representative images of immunohistochemical staining of OCN at the fracture area (A), and quantitative analyses of OCN intensity (B). Scale bars: 50 μ m, or 25 μ m (zoomed). n = 5 per group. C) qRT-PCR analysis of *Runx2*, *Bglap*, and *Col1a* gene expression in fractured bone tissues with different treatments. n = 5 per group. D, E) Representative images of Trap staining (D) and quantitative analyses of the positively stained area at the fracture area (E). Scale bars: 100 μ m or 50 μ m (zoomed). n = 5 per group. * $P < 0.05$.

fracture sites *ex vivo* using a fluorescence tomography imaging system. The results revealed a strong fluorescence signal at the fracture sites of BMSC-aptgel-treated mice after 6 h, in contrast to only a weak fluorescence signal in the Gel- and Rd-aptgel-treated mice (Fig. 3A, upper). After 12 h, fluorescent signals could still be observed at the fracture site of the middle femur in only the BMSC-aptgel-treated mice, while fluorescent signals were hardly detectable in the fracture site of the Gel- and Rd-aptgel-treated mice (Fig. 3A, lower). The quantitative analysis presented that the fluorescence intensity at the fracture site of BMSC-aptgel-treated mice was considerably higher than the Gel- and Rd-aptgel-treated mice at 6 and 12 h (Fig. 3B and C).

The fractured femur underwent immunohistochemical staining of Nestin, a progenitor cell marker [38], to evaluate the number of BMSCs in the fracture site and verify the attraction effect of BMSC-aptgel to endogenous BMSCs further. Controls included Gel, free aqueous Apt, and Rd-aptgel. The results revealed a significant increase in the number of endogenous BMSCs at the fracture site in the BMSC-aptgel-treated mice than the control mice (Fig. 3D and E). These findings confirmed that BMSC-aptgel could attract many BMSCs to the fracture site. Although aptamers are widely used for recognizing, targeting delivery, and other purposes, the specific mechanisms are the present research challenge [39]. We hypothesize that the affinity of BMSC-apt for BMSCs is due to the specific recognition and binding of the aptamers to surface glycoproteins on BMSCs, which may not be present or as effective for other cell types. However, we acknowledge that additional experiments may be necessary to fully validate this mechanism, and we have proposed future studies to further investigate the specificity of BMSC-aptgels for BMSCs.

3.4. BMSC-aptgel accelerates fracture healing *in vivo*

Then, to comprehensively evaluate the effect of BMSC-aptgel on accelerating mouse femoral fracture healing, we expanded our grouping scope. In addition to a control group, a hydrogel group, and a hydrogel group containing a randomly sequenced aptamer, we also included a group with free BMSC-apt alone without the hydrogel. After three weeks, microcomputed tomography (μ CT) coronal and three-dimensional reconstructions of the fracture site demonstrated that the BMSC-aptgel-treated group had significantly more new bone formation (Fig. 4A). At six weeks, the fracture site of the BMSC-aptgel-treated group had almost completely healed, whereas other groups still had visible fracture lines or minor callus formation (Fig. 4E). Newly formed bone tissue was quantified for each group by analyzing the bone volume to tissue volume ratio (BV/TV). Fig. 4B–D and 4F–4H present that the volume of new bone in the BMSC-aptgel group was the highest ($70.63 \pm 9.04\%$ at three weeks and $88.34 \pm 4.12\%$ at six weeks), indicating a continual increase in bone content over time. Additionally, the BMSC-aptgel group demonstrated a significantly greater volume of new bone than the control group ($44.81 \pm 10.34\%$ at three weeks and $71.91 \pm 7.67\%$ at six weeks). Notably, the BV/TV ratio of the PEG gel group ($56.79 \pm 12.82\%$ at three weeks and $80.09 \pm 5.04\%$ at six weeks) trended to be higher than that of the fracture model control group ($44.81 \pm 10.34\%$ at three weeks and $71.91 \pm 7.67\%$ at six weeks), indicating that hydrogels might offer benefits in promoting fracture healing.

Safranin O/fast green (SO/FG) staining revealed significantly lower areas of new bone formation in the Rd-aptgel and control groups relative to the BMSC-aptgel group (Fig. 4I and J). Furthermore, histological analysis with hematoxylin and eosin (H&E) indicated that the BMSC-aptgel group had a significantly higher number of typical new bone volumes than the other groups at three weeks (Fig. 4K). Subsequently, the six-week midfemur underwent a three-point bending test to determine the biomechanical properties of the fractured femur. The maximum bending load of femoral fractures was significantly higher in the BMSC-aptgel group than in the control and Rd-aptgel groups (Fig. 4L). In comparison to traditional biomaterials such as ceramics and biodegradable polymers [40,41], the targeting ability of BMSC-aptgel

allows it to effectively guide BMSCs to the site of bone injury, promoting bone regeneration. Furthermore, compared to biologically active materials like growth factors and cytokines [40,41], BMSC-aptgel demonstrates better biocompatibility, minimizing inflammation responses in the body and reducing the risk of complication. However, we acknowledge that further research is still needed to optimize its performance and validate its clinical effectiveness.

In our mouse femoral fracture model, the results indicated that the BMSC-aptgel notably enhanced the initial formation of new bone and fostered its mineralization progressively. One limitation of our study is the lack of explicit exploration into the fate of BMSC-aptgel during fracture healing. However, based on previous research [24,42] and our experimental results, BMSC-aptgel exhibits excellent sustained loading capabilities and provides adequate physical space to recruit a large number of BMSCs, thus promoting bone regeneration and fracture healing. It can be inferred that during the process of fracture healing, BMSC-aptgel may persist to some extent at the fracture site. However, it is also possible that as new bone tissue forms and grows, it gradually replaces the original BMSC-aptgel. Over time, BMSC-aptgel may undergo gradual degradation and eventual absorption, making way for the newly formed bone tissue.

3.5. BMSC-aptgel enhances osteoblastic differentiation *in vivo*

The fracture repair involves a dynamic balance between osteogenesis and osteoclasts [43,44]. Immunohistochemical staining of osteocalcin (OCN; osteoblast marker) revealed a greater number of osteoblasts at the mid-femoral fracture site in BMSC-aptgel-treated mice (Fig. 5A). The quantitative results also indicated significantly higher levels of OCN staining intensity in BMSC-aptgel-treated mice than in Gel or Rd-aptgel-treated mice (Fig. 5B). Quantitative real-time PCR (qRT-PCR) analysis revealed that treatment with BMSC-aptgel caused a significant increase in the expression of osteogenic factors including *Runx2*, *Bglap*, and *Col1 α* , as compared with the vehicle-treated mice (Fig. 5C). These findings suggested that the BMSCs recruited by the BMSC-aptgel might differentiate into osteoblasts, promoting new bone formation at the fracture site and accelerating healing in mice. However, Trap staining revealed that BMSC-aptgel did not significantly increase the number of osteoclasts on the surface of the trabecular bone at the fracture site compared to Gel and Rd-aptgel-treated mice (Fig. 5D and E). Therefore, the BMSC-aptgel effect on osteoclastic activity *in vivo* was inconsistent with *in vitro* study's results, presenting that BMSC-aptgel promoted osteoclast differentiation.

While BMSC-aptgel has been shown to promote osteoclast activity *in vitro*, this effect is not evident *in vivo*. This could be attributed to the differences in the microenvironments between *in vitro* and *in vivo* systems. In an *in vivo* setting, BMSC-aptgel may be influenced by various factors, such as the inflammatory environment, blood supply, cytokines, etc., which could alter its behavior and function. Additionally, the inherent complexity of *in vivo* experiments may contribute to the divergence from *in vitro* findings. Another possible explanation is the difference in detection time points between *in vivo* and *in vitro* studies. In our *in vivo* experiments, we only assessed the osteoclastic activity by TRAP staining after 3 weeks of treatment, while *in vitro* TRAP staining was performed after 12 days of induction. The osteoclast activity induced by BMSC-aptgel *in vitro* may be transient or require specific conditions that are not present *in vivo*.

3.6. BMSC-aptgel decreases local inflammatory responses *in vivo*

During the process of fracture repair, the inflammatory response is one of the crucial biological processes. Inflammation plays a pivotal role in fracture healing, as it aids in the clearance of necrotic tissue, pathogens, and providing essential growth factors and cytokines for the repair process [29,45]. When a bone fractures, the surrounding soft tissues become damaged and bleed, triggering an inflammatory response that

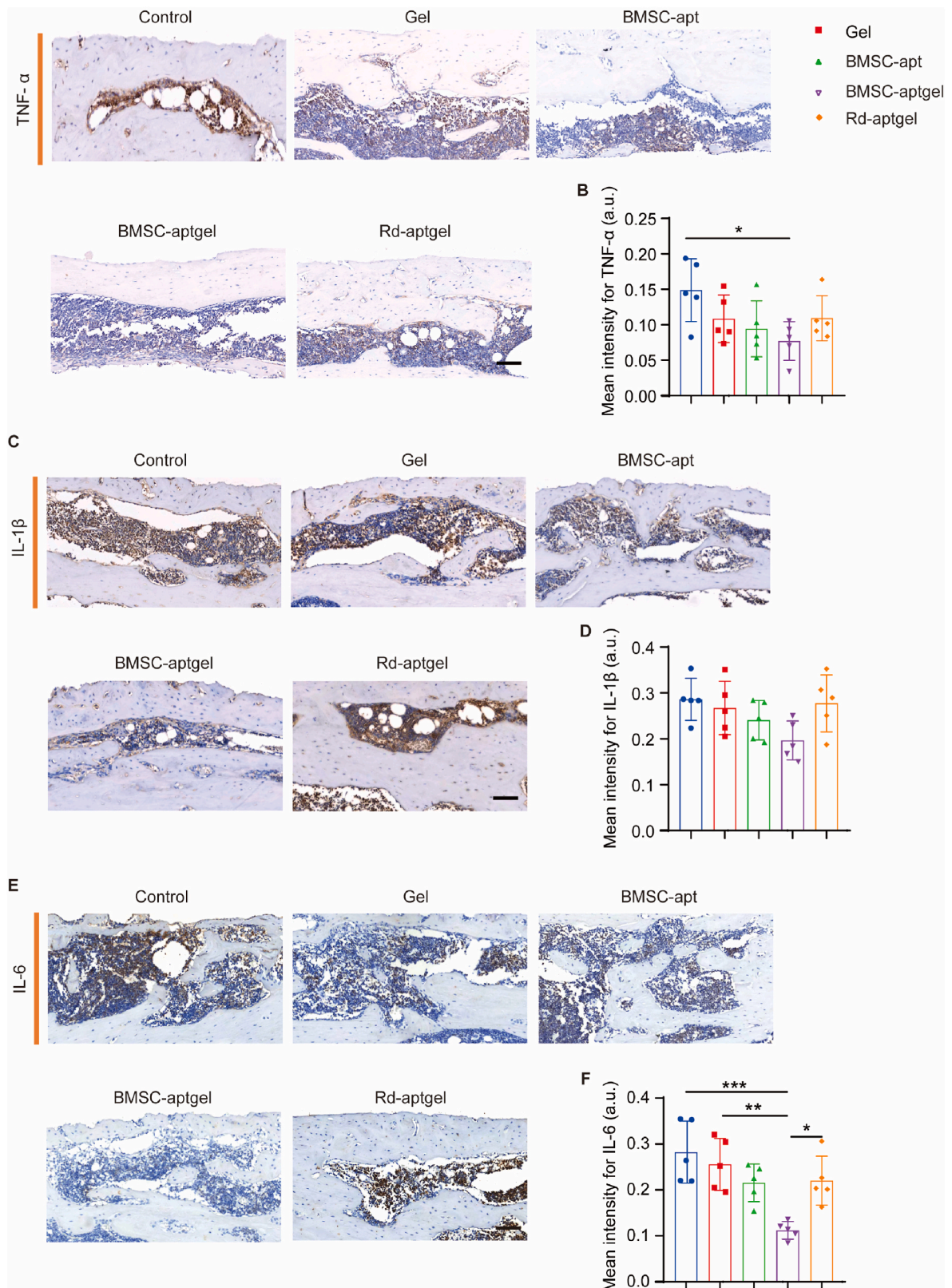


Fig. 6. BMSC-aptgel decreases local inflammatory responses in vivo.

A, C, E) Representative images of immunohistochemical staining of TNF- α (A), IL-1 β (C), and IL-6 (E) in the fracture area. Scale bar: 100 μ m. B, D, F) Quantitative analyses of TNF- α (B), IL-1 β (D), and IL-6 (F) intensity. n = 5 per group. * P < 0.05, ** P < 0.01, *** P < 0.001.

can significantly influence fracture healing [46,47]. However, according to previous studies and our research, excessive inflammation can stimulate osteoclast precursor cell fusion, leading to bone resorption [48–51]. Therefore, understanding how BMSC-aptgel modulates the inflammatory response is of significant importance for optimizing fracture treatment and promoting fracture healing. Multiple studies have confirmed that BMSCs can regulate the immune response and alleviate inflammation via paracrine mechanisms and direct interactions with immune cells, ultimately reducing inflammatory tissue damage [52–55]. Here, the local inflammation levels at the fracture site were measured after three weeks. We discovered that BMSC-aptgel could decrease local inflammatory responses *in vivo*. Immunohistochemical staining of tumor necrosis factor- α (TNF- α ; Fig. 6A and B) and interleukin-6 (IL-6; Fig. 6E and F) in the fracture area displayed significantly lower staining intensity for the BMSC-aptgel group than in other groups. The BMSC-aptgel-treated group had the lowest interleukin-1 beta (IL-1 β) staining intensity, but this difference was not statistically significant (Fig. 6C and D). Notably, the above-mentioned proinflammatory cytokines have previously been shown to impair angiogenesis during fracture healing, thereby affecting fracture healing and bone regeneration [56–58]. These data suggested that BMSCs recruited by BMSC-aptgel regulated the local inflammatory responses at the fracture site, thus leading to a favorable microenvironment for fracture healing.

4. Conclusion

In conclusion, we have developed for the first time a novel strategy based on efficient *in situ* bone regeneration aiming to promote bone repair via PEG hydrogels loaded with aptamers that specifically target BMSCs. We discovered that aptamer-loaded, porous mesh PEG-engineered hydrogels were highly effective in recruiting BMSCs in a homogeneous cellular environment. *In vivo* tracing confirmed the recruitment effect of BMSC-aptgel to BMSCs at the fracture site, also supported by the positive impact of BMSC-aptgel on promoting bone regeneration in the mouse femoral fracture model. The mechanism underlying its efficacy in regulating osteogenic differentiation by BMSCs induces bone regeneration while reducing the local inflammatory response via paracrine effects, resulting in faster fracture healing and mineralization. Therefore, the constructed BMSC-aptgel is a promising carrier for *in situ* bone regeneration and further clinical studies are required for its application. Consequently, we can gain valuable insight into the recruitment of targeted cells. These results promise the future regeneration of other tissues and organs.

Credit author statement

J.-S. Gong and G.-Q. Zhu contributed equally to this work. H. Xie, Z.-X. Wang, and W. Du conceived the project and designed the experiments. J.-S. Gong, G.-Q. Zhu, Y. Zhang, B. Chen, Y.-W. Liu, and J.-T. Zou performed the experiments. H.-M. Li, Z.-H. He, Y.-X. Qian, S. Zhu, X.-Y. Hu, S.-S. Rao, and J. Cao contributed to the experimental technical consultations. J.-S. Gong, G.-Q. Zhu, and Y.-W. Liu contributed to the data acquisition and analysis. H. Xie, Z.-X. Wang, W. Du, and J.-S. Gong wrote the manuscript. All authors reviewed and revised the manuscript.

Declaration of competing interest

The authors declare that they have no known competing financial interests or personal relationships that could have appeared to influence the work reported in this paper.

Data availability

Data will be made available on request.

Acknowledgements

This work was supported by the National Natural Science Foundation of China (82125023, 82072504 to H. X.; 82272562 to Z.-X. W.), the Hunan Province Natural Science Foundation of China (2023JJ30872 to W. D.).

References

- [1] H. Lin, J. Sohn, H. Shen, M.T. Langhans, R.S. Tuan, Bone marrow mesenchymal stem cells: aging and tissue engineering applications to enhance bone healing, *Biomaterials* 203 (2019) 96–110, <https://doi.org/10.1016/j.biomaterials.2018.06.026>.
- [2] F. Shang, Y. Yu, S. Liu, L. Ming, Y. Zhang, Z. Zhou, J. Zhao, Y. Jin, Advancing application of mesenchymal stem cell-based bone tissue regeneration, *Bioact. Mater.* 6 (2021) 666–683, <https://doi.org/10.1016/j.bioactmat.2020.08.014>.
- [3] S. Gur-Cohen, H. Yang, S.C. Baksh, Y. Miao, J. Levorso, R.P. Kataru, X. Liu, J. de la Cruz-Racelis, B.J. Mehrara, E. Fuchs, Stem cell-driven lymphatic remodeling coordinates tissue regeneration, *Science* 366 (2019) 1218–1225, <https://doi.org/10.1126/science.aay4509>.
- [4] A. Julien, A. Kanagalingam, E. Martínez-Sarrà, J. Megret, M. Luka, M. Ménager, F. Relaix, C. Colnot, Direct contribution of skeletal muscle mesenchymal progenitors to bone repair, *Nat. Commun.* 12 (2021) 2860, <https://doi.org/10.1038/s41467-021-22842-5>.
- [5] E. Anitua, M. Sánchez, G. Orive, Potential of endogenous regenerative technology for *in situ* regenerative medicine, *Adv. Drug Deliv. Rev.* 62 (2010) 741–752, <https://doi.org/10.1016/j.addr.2010.01.001>.
- [6] J.R. Dias, N. Ribeiro, S. Baptista-Silva, A.R. Costa-Pinto, N. Alves, A.L. Oliveira, *In situ* enabling approaches for tissue regeneration: current challenges and new developments, *Front. Bioeng. Biotechnol.* 8 (2020) 85, <https://doi.org/10.3389/fbioe.2020.00085>.
- [7] B.D. Sui, C.H. Hu, A.Q. Liu, C.X. Zheng, K. Xuan, Y. Jin, Stem cell-based bone regeneration in diseased microenvironments: challenges and solutions, *Biomaterials* 196 (2019) 18–30, <https://doi.org/10.1016/j.biomaterials.2017.10.046>.
- [8] M. Ullah, D.D. Liu, A.S. Thakor, Mesenchymal stromal cell homing: mechanisms and strategies for improvement, *iScience* 15 (2019) 421–438, <https://doi.org/10.1016/j.isci.2019.05.004>.
- [9] H. Sun, Q. Guo, C. Shi, R.H. McWilliam, J. Chen, C. Zhu, F. Han, P. Zhou, H. Yang, J. Liu, X. Sun, B. Meng, W. Shu, B. Li, CD271 antibody-functionalized microspheres capable of selective recruitment of reparative endogenous stem cells for *in situ* bone regeneration, *Biomaterials* 280 (2022), 121243, <https://doi.org/10.1016/j.biomaterials.2021.121243>.
- [10] J. Bai, G. Ge, Q. Wang, W. Li, K. Zheng, Y. Xu, H. Yang, G. Pan, D. Geng, Engineering stem cell recruitment and osteoinduction via bioadhesive molecular mimics to improve osteoporotic bone-implant integration, *Research* 2022 (2022), 9823784, <https://doi.org/10.34133/2022/9823784>.
- [11] Y. Safarova, B. Umbayev, G. Hortelano, S. Askarova, Mesenchymal stem cells modifications for enhanced bone targeting and bone regeneration, *Regen. Med.* 15 (2020) 1579–1594, <https://doi.org/10.2217/rme-2019-0081>.
- [12] Y. Chen, Y. Li, F. Lu, Z. Dong, Endogenous bone marrow-derived stem cell mobilization and homing for *in situ* tissue regeneration, *Stem Cell.* 41 (2023) 541–551, <https://doi.org/10.1093/stmcls/sxad026>.
- [13] H. Sun, Q. Guo, C. Shi, R.H. McWilliam, J. Chen, C. Zhu, F. Han, P. Zhou, H. Yang, J. Liu, X. Sun, B. Meng, W. Shu, B. Li, CD271 antibody-functionalized microspheres capable of selective recruitment of reparative endogenous stem cells for *in situ* bone regeneration, *Biomaterials* 280 (2022), 121243, <https://doi.org/10.1016/j.biomaterials.2021.121243>.
- [14] C.H. Kim, H.E. Broxmeyer, *In vitro* behavior of hematopoietic progenitor cells under the influence of chemoattractants: stromal cell-derived factor-1, steel factor, and the bone marrow environment, *Blood* 91 (1998) 100–110, <https://doi.org/10.1182/blood.V91.1.100>.
- [15] H. Zhang, X. Li, J. Li, L. Zhong, X. Chen, S. Chen, SDF-1 mediates mesenchymal stem cell recruitment and migration via the SDF-1/CXCR4 axis in bone defect, *J. Bone Miner. Metabol.* 39 (2021) 126–138, <https://doi.org/10.1007/s00774-020-01122-0>.
- [16] S. Liu, Y. Liu, L. Jiang, Z. Li, S. Lee, C. Liu, J. Wang, J. Zhang, Recombinant human BMP-2 accelerates the migration of bone marrow mesenchymal stem cells via the CDC42/PAK1/LIMK1 pathway *in vitro* and *in vivo*, *Biomater. Sci.* 7 (2018) 362–372, <https://doi.org/10.1039/c8bm00846a>.
- [17] W. Zhang, N. Wang, M. Yang, T. Sun, J. Zhang, Y. Zhao, N. Huo, Z. Li, Periosteum and development of the tissue-engineered periosteum for guided bone regeneration, *Journal of Orthopaedic Translation* 33 (2022) 41–54, <https://doi.org/10.1016/j.jot.2022.01.002>.
- [18] X. Chen, L. Zhang, X.Y. Shao, W. Gong, T.S. Shi, J. Dong, Y. Shi, S.Y. Shen, Y. He, J. H. Qin, J. Lu, Q. Jiang, B.S. Guo, Specific clearance of senescent synoviocytes suppresses the development of osteoarthritis based on aptamer-functionalized targeted drug delivery system, *Adv. Funct. Mater.* 32 (2022), 2109460, <https://doi.org/10.1002/adfm.202109460>.
- [19] P. Röthlisberger, M. Hollenstein, Aptamer chemistry, *Adv. Drug Deliv. Rev.* 134 (2018) 3–21, <https://doi.org/10.1016/j.addr.2018.04.007>.

- [20] J. Yuhan, L. Zhu, L. Zhu, K. Huang, X. He, W. Xu, Cell-specific aptamers as potential drugs in therapeutic applications: a review of current progress, *J. Contr. Release* 346 (2022) 405–420, <https://doi.org/10.1016/j.jconrel.2022.04.039>.
- [21] G. Zhu, X. Chen, Aptamer-based targeted therapy, *Adv. Drug Deliv. Rev.* 134 (2018) 65–78, <https://doi.org/10.1016/j.addr.2018.08.005>.
- [22] B. Kong, Y. Chen, R. Liu, X. Liu, C. Liu, Z. Shao, L. Xiong, X. Liu, W. Sun, S. Mi, Fiber reinforced GelMA hydrogel to induce the regeneration of corneal stroma, *Nat. Commun.* 11 (2020) 1435, <https://doi.org/10.1038/s41467-020-14887-9>.
- [23] R. Zhong, S. Talebian, B. Mendes, G. Wallace, R. Langer, J. Conde, J. Shi, Hydrogels for RNA delivery, *Nat. Mater.* 22 (2023) 818–831, <https://doi.org/10.1038/s41563-023-01472-w>.
- [24] S.F. Enam, J.R. Krieger, T. Saxena, B.E. Watts, C.E. Olingy, E.A. Botchwey, R. V. Bellamkonda, Enrichment of endogenous fractalkine and anti-inflammatory cells via aptamer-functionalized hydrogels, *Biomaterials* 142 (2017) 52–61, <https://doi.org/10.1016/j.biomaterials.2017.07.013>.
- [25] C.J. Li, P. Cheng, M.K. Liang, Y.S. Chen, Q. Lu, J.Y. Wang, Z.Y. Xia, H.D. Zhou, X. Cao, H. Xie, E.Y. Liao, X.H. Luo, MicroRNA-188 regulates age-related switch between osteoblast and adipocyte differentiation, *J. Clin. Investig.* 125 (2015) 1509–1522, <https://doi.org/10.1172/jci77716>.
- [26] Z. Luo, F. Li, Y. Liu, S. Rao, H. Yin, J. Huang, C. Chen, Y. Hu, Y. Zhang, Y. Tan, L. Yuan, T. Chen, H. Liu, J. Cao, Z. Liu, Z. Wang, H. Xie, Aptamer-functionalized exosomes from bone marrow stromal cells target bone to promote bone regeneration, *Nanoscale* 11 (2019) 20884–20892, <https://doi.org/10.1039/c9nr02791b>.
- [27] T.H. Ambrosi, O. Marecic, A. McArdle, R. Sinha, G.S. Gulati, X. Tong, Y. Wang, H. M. Steininger, M.Y. Hoover, L.S. Koepke, M.P. Murphy, J. Sokol, E.Y. Seo, R. Tevlin, M. Lopez, R.E. Brewer, S. Mascharak, L. Lu, O. Ajanaku, S.D. Conley, J. Seita, M. Morri, N.F. Neff, D. Sahoo, F. Yang, I.L. Weissman, M.T. Longaker, C.K. F. Chan, Aged skeletal stem cells generate an inflammatory degenerative niche, *Nature* 597 (2021) 256–262, <https://doi.org/10.1038/s41586-021-03795-7>.
- [28] X. Mao, R. Cheng, H. Zhang, J. Bae, L. Cheng, L. Zhang, L. Deng, W. Cui, Y. Zhang, H.A. Santos, X. Sun, Self-healing and injectable hydrogel for matching skin flap regeneration, *Adv. Sci.* 6 (2019), 1801555, <https://doi.org/10.1002/adv.201801555>.
- [29] I. Yadav, S.D. Purohit, H. Singh, N. Das, P. Roy, N.C. Mishra, A highly transparent tri-polymer complex in situ hydrogel of HA, collagen and four-arm-PEG as potential vitreous substitute, *Biomed. Mater.* 16 (2021), 065018, <https://doi.org/10.1088/1748-605X/ac2714>.
- [30] A. Bharadwaz, A.C. Jayasuriya, Recent trends in the application of widely used natural and synthetic polymer nanocomposites in bone tissue regeneration, *Materials science & engineering, C, Materials for Biological Applications* 110 (2020), 110698.
- [31] J.R. Yang, H.M. He, D. Li, Q. Zhang, L.Z. Xu, C.S. Ruan, Advanced strategies in the application of gelatin-based bioink for extrusion bioprinting, *Bio-Design and Manufacturing* 6 (2023) 586–608, <https://doi.org/10.1007/s42242-023-00236-4>.
- [32] A. D'Souza, A. R. Shegokar, Polyethylene glycol (PEG): a versatile polymer for pharmaceutical applications, *Expet Opin. Drug Deliv.* 13 (2016) 1257–1275, <https://doi.org/10.1080/17425247.2016.1182485>.
- [33] J. Wang, F. Zhang, W.P. Tsang, C. Wan, C. Wu, Fabrication of injectable high strength hydrogel based on 4-arm star PEG for cartilage tissue engineering, *Biomaterials* 120 (2017) 11–21, <https://doi.org/10.1016/j.biomaterials.2016.12.015>.
- [34] H. Liu, Y. Du, J.P. St-Pierre, M.S. Bergholt, H. Autefage, J. Wang, M. Cai, G. Yang, M.M. Stevens, S. Zhang, Bioenergetic-active materials enhance tissue regeneration by modulating cellular metabolic state, *Sci. Adv.* 6 (2020), eaay7608, <https://doi.org/10.1126/sciadv.aay7608>.
- [35] Y. Ju, Y. Hu, P. Yang, X. Xie, B. Fang, Extracellular vesicle-loaded hydrogels for tissue repair and regeneration, *Materials Today, Bio* 18 (2023), 100522, <https://doi.org/10.1016/j.mtbio.2022.100522>.
- [36] Accelerated surgery versus standard care in hip fracture (HIP ATTACK): an international, randomised, controlled trial, *Lancet* 395 (2020) 698–708, [https://doi.org/10.1016/s0140-6736\(20\)30058-1](https://doi.org/10.1016/s0140-6736(20)30058-1).
- [37] K. Man, M.Y. Brunet, M. Fernandez-Rhodes, S. Williams, L.M. Heaney, L. A. Gethings, A. Federici, O.G. Davies, D. Hoey, S.C. Cox, Epigenetic reprogramming enhances the therapeutic efficacy of osteoblast-derived extracellular vesicles to promote human bone marrow stem cell osteogenic differentiation, *J. Extracell. Vesicles* 10 (2021), e12118, <https://doi.org/10.1002/jev2.12118>.
- [38] J. Calderaro, L. Di Tommaso, P. Maillé, A. Beaufrère, C.T. Nguyen, L. Heij, V. Gnemmi, R.P. Graham, F. Charlotte, S. Chartier, D. Wendum, M. Vij, D. Allende, A. Diaz, C. Fuster, B. Rivière, A. Herrero, J. Augustin, K. Evert, D.F. Calvisi, W. Q. Leow, H.H.W. Leung, J. Bednarsch, E. Boleslawski, M. Rela, A.W. Chan, A. Forner, M. Reig, A. Pujals, L. Favre, M. Allaire, O. Scatton, A. Uguen, E. Trépo, L. O. Sanchez, D. Chatelain, M. Rimmelink, C. Boulagnon-Rombi, C. Bazille, N. Sturm, B. Menahem, E. Frouin, D. Tougeron, C. Tournigand, E. Kempf, H. Kim, M. Ningarhari, S. Michalak-Provost, J.N. Kather, A.S.H. Gouw, P. Gopal, R. Brustia, E. Vibert, K. Schulze, D.F. Rütger, S.A. Weidemann, R. Rhaïem, J.C. Nault, A. Laurent, G. Amaddeo, H. Regnault, E. de Martin, C. Sempoux, P. Navale, J. Shinde, K. Bacchuwar, M. Westerhoff, R.C. Lo, M. Sebbagh, C. Guettier, M. Lequoy, M. Komuta, M. Zioli, V. Paradis, J. Shen, S. Caruso, Nestin as a diagnostic and prognostic marker for combined hepatocellular-cholangiocarcinoma, *J. Hepatol.* 77 (2022) 1586–1597, <https://doi.org/10.1016/j.jhep.2022.07.019>.
- [39] G. Zhu, X. Chen, Aptamer-based targeted therapy, *Adv. Drug Deliv. Rev.* 134 (2018) 65–78, <https://doi.org/10.1016/j.addr.2018.08.005>.
- [40] W. Wang, K.W.K. Yeung, Bone grafts and biomaterials substitutes for bone defect repair: a review, *Bioact. Mater.* 2 (2017) 224–247, <https://doi.org/10.1016/j.bioactmat.2017.05.007>.
- [41] S. Wei, J.X. Ma, L. Xu, X.S. Gu, X.L. Ma, Biodegradable materials for bone defect repair, *Military Medical Research* 7 (2020) 54, <https://doi.org/10.1186/s40779-020-00280-6>.
- [42] X. Wang, X. Song, T. Li, J. Chen, G. Cheng, L. Yang, C. Chen, Aptamer-functionalized bioscaffold enhances cartilage repair by improving stem cell recruitment in osteochondral defects of rabbit knees, *Am. J. Sports Med.* 47 (2019) 2316–2326, <https://doi.org/10.1177/0363546519856355>.
- [43] K.K. Sivaraj, P.G. Majev, H.W. Jeong, B. Dharmalingam, D. Zeuschner, S. Schröder, M.G. Bixel, M. Timmen, R. Stange, R.H. Adams, Mesenchymal stromal cell-derived septoclasts resorb cartilage during developmental ossification and fracture healing, *Nat. Commun.* 13 (2022) 571, <https://doi.org/10.1038/s41467-022-28142-w>.
- [44] Z.Y. Huang, Z.F. Tian, M. Zhu, C.T. Wu, Y.F. Zhu, Recent advances in biomaterial scaffolds for integrative tumor therapy and bone regeneration, *Advanced Therapeutics* 4 (2021), 2000212, <https://doi.org/10.1002/adtp.202000212>.
- [45] D. Clark, S. Brazina, F. Yang, D. Hu, C.L. Hsieh, E.C. Niemi, T. Miclau, M. C. Nakamura, R. Marcucio, Age-related changes to macrophages are detrimental to fracture healing in mice, *Aging Cell* 19 (2020), e13112, <https://doi.org/10.1111/acel.13112>.
- [46] L. Claes, S. Recknagel, A. Ignatius, Fracture healing under healthy and inflammatory conditions, *Nat. Rev. Rheumatol.* 8 (2012) 133–143, <https://doi.org/10.1038/nrrheum.2012.1>.
- [47] T.A. Einhorn, L.C. Gerstenfeld, Fracture healing: mechanisms and interventions, *Nat. Rev. Rheumatol.* 11 (2015) 45–54, <https://doi.org/10.1038/nrrheum.2014.164>.
- [48] H. Byun, G. Jang, M. Hong, J. Yeo, H. Shin, W. Kim, H. Shin, Biomimetic anti-inflammatory and osteogenic nanoparticles self-assembled with mineral ions and tannic acid for tissue engineering, *Nano Convergence* 9 (2022) 47, <https://doi.org/10.1186/s40580-022-00338-2>.
- [49] W. Zhou, Z. Lin, Y. Xiong, H. Xue, W. Song, T. Yu, L. Chen, Y. Hu, A.C. Panayi, Y. Sun, F. Cao, G. Liu, L. Hu, C. Yan, X. Xie, W. Qiu, B. Mi, G. Liu, Dual-targeted nanopatform regulating the bone immune microenvironment enhances fracture healing, *ACS Appl. Mater. Interfaces* 13 (2021) 56944–56960, <https://doi.org/10.1021/acami.1c17420>.
- [50] S.S. Rao, Y. Hu, P.L. Xie, J. Cao, Z.X. Wang, J.H. Liu, H. Yin, J. Huang, Y.J. Tan, J. Luo, M.J. Luo, S.Y. Tang, T.H. Chen, L.Q. Yuan, E.Y. Liao, R. Xu, Z.Z. Liu, C. Y. Chen, H. Xie, Omentin-1 prevents inflammation-induced osteoporosis by downregulating the pro-inflammatory cytokines, *Bone Research* 6 (2018) 9, <https://doi.org/10.1038/s41413-018-0012-0>.
- [51] Z.W. Luo, P.P. Liu, Z.X. Wang, C.Y. Chen, H. Xie, Macrophages in osteosarcoma immune microenvironment: implications for immunotherapy, *Front. Oncol.* 10 (2020), 586580, <https://doi.org/10.3389/fonc.2020.586580>.
- [52] J. Pajarinen, T. Lin, E. Gibon, Y. Kohno, M. Maruyama, K. Nathan, L. Lu, Z. Yao, S. B. Goodman, Mesenchymal stem cell-macrophage crosstalk and bone healing, *Biomaterials* 196 (2019) 80–89, <https://doi.org/10.1016/j.biomaterials.2017.12.025>.
- [53] L. Mazini, L. Rochette, B. Admou, S. Amal, G. Malka, Hopes and limits of adipose-derived stem cells (ADSCs) and mesenchymal stem cells (MSCs) in wound healing, *Int. J. Mol. Sci.* 21 (2020) 1306, <https://doi.org/10.3390/ijms21041306>.
- [54] Y. Shi, Y. Wang, Q. Li, K. Liu, J. Hou, C. Shao, Y. Wang, Immunoregulatory mechanisms of mesenchymal stem and stromal cells in inflammatory diseases, *Nat. Rev. Nephrol.* 14 (2018) 493–507, <https://doi.org/10.1038/s41581-018-0023-5>.
- [55] A. Najj, M. Eitoku, B. Favier, F. Deschaseaux, N. Rouas-Freiss, N. Suganuma, Biological functions of mesenchymal stem cells and clinical implications, *Cell. Mol. Life Sci.* 76 (2019) 3323–3348, <https://doi.org/10.1007/s00018-019-03125-1>.
- [56] D. Cici, A. Corrado, C. Rotondo, F.P. Cantatore, Wnt signaling and biological therapy in rheumatoid arthritis and spondyloarthritis, *Int. J. Mol. Sci.* 20 (2019) 5552, <https://doi.org/10.3390/ijms20225552>.
- [57] M. Lo Monaco, P. Gervois, J. Beaumont, P. Clegg, A. Bronckers, J.M. Vandewerd, I. Lambrichts, Therapeutic potential of dental pulp stem cells and leukocyte- and platelet-rich fibrin for osteoarthritis, *Cells* 9 (2020) 980, <https://doi.org/10.3390/cells9040980>.
- [58] T. Wang, C. He, Pro-inflammatory cytokines: the link between obesity and osteoarthritis, *Cytokine Growth Factor Rev.* 44 (2018) 38–50, <https://doi.org/10.1016/j.cytogfr.2018.10.002>.